Journal of
Materials Chemistry A

Accepted Manuscript

This is an *Accepted Manuscript*, which has been through the RSC Publishing peer review process and has been accepted for publication.

Accepted Manuscripts are published online shortly after acceptance, which is prior to technical editing, formatting and proof reading. This free service from RSC Publishing allows authors to make their results available to the community, in citable form, before publication of the edited article. This *Accepted Manuscript* will be replaced by the edited and formatted *Advance Article* as soon as this is available.

To cite this manuscript please use its permanent Digital Object Identifier (DOI®), which is identical for all formats of publication.

More information about *Accepted Manuscripts* can be found in the **Information for Authors**.

Please note that technical editing may introduce minor changes to the text and/or graphics contained in the manuscript submitted by the author(s) which may alter content, and that the standard **Terms & Conditions** and the **ethical guidelines** that apply to the journal are still applicable. In no event shall the RSC be held responsible for any errors or omissions in these *Accepted Manuscript* manuscripts or any consequences arising from the use of any information contained in them.

Journal of Materials Chemistry A RSCPublishing

ARTICLE

High Performance Cr, N - Codoped Mesoporous TiO_2 Microspheres for Lithium-ion Batteries

Cite this: DOI: 10.1039/x0xx00000x

Zhonghe Bi,[*] M. Parans Paranthaman,[*] Bingkun Guo, Raymond R. Unocic, Harry M Meyer III, Craig A Bridges,[*] Xiao-Guang Sun, and Sheng Dai

Received ooth January 2012,
Accepted ooth January 2012

DOI: 10.1039/x0xx00000x

www.rsc.org/

Cr, N-codoped TiO_2 mesoporous microspheres has been successfully synthesized by a facile hydrothermal reaction followed by annealing under ammonia atmosphere. Through introduction of Cr, the Nitrogen doping level was increased from 2.81 at. % for N-doped TiO_2 to 5.68 at. % for Cr, N-codoped TiO_2, which improves the electrical conductivity of TiO_2. When used as an anode for lithium-ion rechargeable batteries, the Cr, N-codoping TiO_2 microspheres led to an enhanced performance of 159.6 $mAhg^{-1}$ at 5 C with a drop of less than 1% after 300 cycles.

Introduction

In recent years, TiO_2 has been identified as one of the most promising materials for electronic devices, solar cell and Li-ion rechargeable batteries (LIBs), as it is found in relatively high abundance in nature, exhibits very low toxicity, and is considered safe.[1] In particular for advanced energy storage systems such as lithium ion batteries, the different polymorphs of TiO_2 (e.g. Anatase, Rutile and TiO_2-B) have been widely investigated as anode materials since there is no formation of SEI (solid electrolyte interface) during charge and discharge.[2] However, its intrinsic physicochemical property of low electronic conductivity leads to a relatively poor rate capability owing to the poor electron transport when utilized as a host for Li-ion intercalation, which limits its practical industrial application. Recently many efforts have been made to solve the problem of poor rate capability of TiO_2 electrodes. One effective method is to reduce the diffusion distance for Li^+ ions by using nanostructured TiO_2, such as nano particles,[3] nanotubes,[4] nanowires,[5] and nanoribbons.[6] Recently promising materials with a mesoporous spherical morphology have been widely reported as electrode materials for Li-ion rechargeable batteries, and micrometer-sized mesoporous spheres have been considered as the optimal material morphology in conventional electrode fabrication due to the high contact area between electrolyte and electrode, short diffusion distance for Li^+ transport, good accommodation of strain during cycling, as well as high packing density.[7] However, one concern for mesoporous materials is the long transport distance of electrons in micron-sized particles, especially for low conducting materials such as TiO_2. Therefore, improving the electronic conductivity of TiO_2 becomes particularly important for micro-sized powders. One approach to achieve this is the use of conducting agents including carbon, metals, and inorganic/organic compounds that have been introduced into TiO_2 particles by coating, mixing, embedding, and reactive chemical/physical methods.[8] However, these methods typically cannot provide a continuous, uniform electron transport path that covers the entire surface of the particles. Another effective approach to increase the electronic conductivity is to modify the bandgap of a pure TiO_2 by different doping schemes to attain enhancement of $[Vo^{\cdot\cdot}]$ and $[h^{\cdot}]$ (electrons or holes). For example, the use of Fe-, W- Nb-, or N-, doped TiO_2 nanoparticles and nanotubes as anode materials for LIBs, which have been confirmed to exhibit improved capacity and rate capability.[9] However, a challenging obstacle is presented by the fundamental limitations in thermodynamic solubility for substitutional doping of TiO_2; the solubility is extremely low for most dopants, which may be of no help in providing mobile charge carriers if the dopants are mainly located at undesirable interstitial sites.[10] Recently a noncompensated n-p co-doping concept has been reported to enhance the visible-light photoactivity of TiO_2 by narrowing its band gap.[11] So far, only two codopant pairs including C-N and F-N have been reported for TiO_2 nanoparticles as anode materials in LIBs.[12] According to our previous study,[11] Cr-N is predicted to be the preferred codopant pair on the basis of first-principle calculations. Furthermore, according to detailed experimental investigations, Cr, N-codoped TiO_2 nanoparticles prepared using wet chemical methods indeed exhibited substantially narrowed band gaps, as well as dramatically enhanced photoabsorption and photoactivity in the visible spectral region.[13] Therefore, it is highly desirable to develop a Cr, N-codoped TiO_2 powder that could combine the advantages of the mesoporous structure, spherical morphology, and higher electronic conductivity.

Herein, we present a facile synthesis of Cr, N-codoped mesoporous TiO_2 microspheres with enhanced electrical conductivity as high power anode materials for LIBs, which exhibit high capacity, good cycling performance, and high rate capability. Initially, the Cr-doped TiO_2 mesoporous microspheres were synthesized via a facile surfactant-free hydrothermal reaction method, and they were thermally treated under a flowing NH_3 atmosphere to attain Cr, N-codoped mesoporous TiO_2 microspheres. This unique microstructure involves micrometer-sized particles with an average diameter near 1.5 μm, containing uniform mesopores of ~ 14 nm, and with spheres composed of agglomerated nanosized crystal grains of 20 nm average size. Due to the improvement in electrical conductivity and

defects after Cr, N-co-doping, the co-doped microspheres display a higher capacity than N-doped TiO_2 microspheres under the same electrode fabrication and test conditions, and exhibit much better rate performance results of 153 $mAhg^{-1}$ at 5 C and 127 $mAhg^{-1}$ at 10 C.

Experimental

Materials preparation: The mesoporous TiO_2 and Cr-doped TiO_2 microspheres were obtained by hydrothermal reaction method without the use of surfactants.[7,9] The process of synthesis was as follows: 25 mmol of urea ($(NH_2)_2CO$, 98+% Alfa) were dissolved in 1.5 mL of deionized water (DI water) and 8.5 mL of ethanol under stirring. Titanium trichloride (5 mmol; 20% $TiCl_3$ in 3% HCl, Alfa) with (for Cr-doped TiO_2) and without (for pure TiO_2) 0.25 mmol of $Cr(NO_3)_3{\cdot}9H_2O$ (98.5%, Alfa) was then added to this solution and stirred for 12 h. The solution was then transferred into a Teflon-lined autoclave and heated to 180°C for 12 h with a heating/cooling rate of 1.0 °C/min. The resulting slurry was filtered and washed with DI water, and then dried in a vacuum oven at 100 °C. The powder was finally heated at 500 °C in air for 5 h to obtain a crystalline, high surface area TiO_2 and 5mol%Cr-doped TiO_2 powders. N-doped and Cr, N-codoped TiO_2 spheres were obtained through annealing pure or Cr-doped TiO_2 under NH_3 gas at 550 °C, with a NH_3 flow rate of 100 ml/min, for 12 h.

Materials characterization: The products were characterized by X-ray diffraction (XRD, Scintag and PANalytical instruments) using Cu Kα radiation and X-ray photoelectron spectroscopy (XPS) (Thermo Scientific K-Alpha XPS system). Rietveld refinement of XRD patterns was performed using the General Structure Analysis System (GSAS) software and the ExpGUI interface.[14] Nitrogen adsorption-desorption isotherms were performed using a TriStar surface area & porosity analyser at 77K. The specific surface area was calculated by the Brunauer-Emmett-Teller (BET) method. The pore size distribution was attained by the Barret-Joyner-Halenda (BJH) method. The microstructural characterization of TiO_2 mesoporous microspheres was performed using a Hitachi HF-3300 S/TEM instrument which was operated at 300 kV.

Evaluation of electrochemical properties: The electrodes were fabricated using the N-doped and Cr, N-codoped TiO_2 microspheres as the active materials, mixed with conductive carbon black and polyvinylidene fluoride (PVDF) binder in a weight ratio of 70:20:10. The slurry was formed with N-methyl-2pyrrolidone (NMP) and coated on a copper foil and dried overnight in a vacuum oven at 120°C. The loading of the electrode was ~2.0 $mgcm^{-2}$. Coin-type half cells (CR2032) were fabricated to evaluate the electrochemical performances of the doped TiO_2 microspheres, using lithium metal as the counter electrode, Celgard 2325 as the separator and $LiPF_6$ (1M) in ethylene carbonate/dimethyl carbonate/diethyl carbonate (EC/DMC/DEC, 1:1:1 vol. %) as the electrolyte. The coin cells were tested using a battery analyzer (Arbin BT2000 charger) and a Princeton Applied Research VersaSTAT 4 potentiostat.

Results and discussion

The X-ray diffraction (XRD) patterns of the pure and doped TiO_2 microspheres are shown in Fig.1. All the main reflections both from pure and doped TiO_2 spheres could be indexed based on the anatase TiO_2 phase (JCPDS No. 84-1286). For N-doped and Cr,N-codoped samples, a very tiny peak at 42.5° was observed, which is from Ti_xN (x=0.76~0.9). There are also small amount of unknown impurities in TiO_2 and N-doped TiO_2 samples. However, all XRD patterns were able to be refined in the anatase phase (space group I 41/a). A

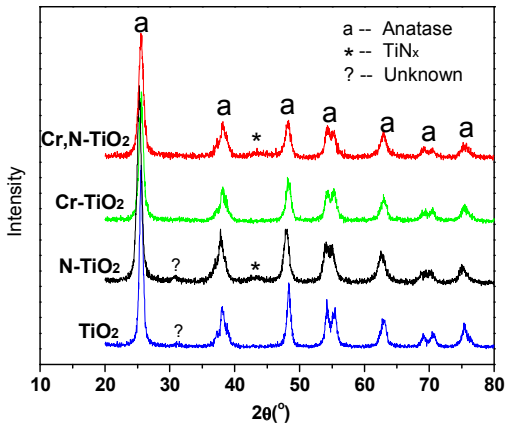

Fig. 1 Room temperature powder X-ray diffraction patterns of pure and doped TiO_2 microspheres.

representative Rietveld refinement of XRD data for the Cr, N-codoped sample is shown in Electronic Supplementary Information (ESI) Figure S1. Relative good agreement between the measured and calculated profile based upon anatase phase Rietveld refinement was observed and the unit cell parameters of the doped and undoped samples could be obtained from the refinements and reported in Table S1. It can be seen that cell parameters *a* and *b* increase with Cr-, N-, or Cr, N- doping, while parameter *c* decreases accordingly. Interestingly, there is little or no change in volume within error, despite the significant change in lattice parameters, suggesting the lattice is undergoing a slight distortion to accommodate the doping. No Cr-relative impurity was observed for TiO_2 substituted by 5 mol% Cr in Cr-doped and Cr,N-codoped samples under our experimental conditions. After ammonolysis, no TiO_xN_y phase was observed from XRD patterns of the N- and Cr, N- doped TiO_2 except very little Ti_xN. However, it is possible that a thin amorphous TiO_xN_y layer was formed on the surface that is not visible to XRD, in addition to nitrogen doping into the bulk.[9]

Figure 2 (c) shows the SEM image of Cr-doped TiO_2 mesoporous microspheres. Compared to the SEM images of pure TiO_2 spheres (as shown in Figure 2 (a) and (b)) reported previously,[9] the size and morphology of the microspheres is retained after doped with 5 mol% Cr. Figure 2 (d) shows the TEM image of Cr, N-codoped TiO_2 microspheres. From Figure 2 (a) and (b), it is clearly seen that the undoped TiO_2 mesoporous microspheres with a typical diameter of 1.5 μm are composed of mesopores and nano-sized crystal grains of ~ 20 nm sizes. Nitrogen isothermal adsorption-desorption measurements were performed to determine the Brunauer-Emmett-Teller (BET) surface area and the porosity of the mesoporous microspheres. The isotherm curves of the undoped and doped TiO_2 microspheres are given in Figure S2, all of which are typical type IV isotherms representing a mesoporous structure, and Cr-doped TiO_2 shows the highest BET specific surface area of 194 m^2g^{-1}, which is higher than that of pure TiO_2 samples ~171 m^2g^{-1}. After Nitride of pure and Cr-doped TiO_2, both of them display similar BET specific surface areas

of 83 and 94 m^2g^{-1}, for N- and Cr, N-doped TiO_2, respectively, which are clearly lower than before nitridated due to sintered at higher temperature (550°C) for longer time (12 h) The pore size distribution is also shown in the Figure S2 inset, and displays an unimodal peak around 12 nm for both pure TiO_2 and Cr-doped TiO_2, which increase to around 14 nm for both N-doped TiO_2 and Cr, N-doped TiO_2.

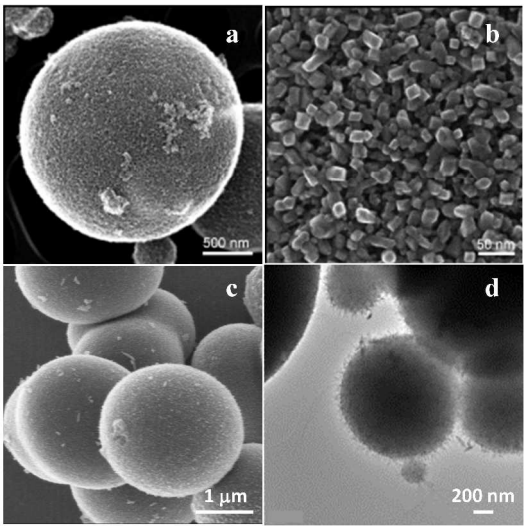

Fig. 2 (a) and (b) SEM images of undoped TiO_2 mesoporous microspheres, (c) SEM image of Cr-doped TiO_2 mesoporous microspheres, and (d) TEM image of Cr, N-codoped mesoporous microspheres.

X-ray photoelectron spectroscopy (XPS) analysis was carried out to determine the composition and identify the valence states of the N- and Cr, N-doped TiO_2 microspheres. The high-resolution XPS results are presented in Figure 3. Although the coincidence of the Cr spectra and Ti2s plasmon loss satellites at ~566 and ~579 eV is an important consideration, the Cr2p core level spectrum does clearly indicate the presence of Cr^{3+} dopant ions inside the TiO_2 microspheres given that the peaks at ~587 eV and ~577 eV (Cr2p components) were clearly observed in the spectra of the Cr-doped TiO_2 and Cr, N-codoped TiO_2 microspheres.[15] However, for the samples without Cr-doping only one peak at ~577 eV was observed, due to Ti2s, and the intensity of this peak was lower than in TiO_2 with Cr-doping.[16] In Cr, N-codoped TiO_2, no peak at ~574.5 eV from Cr-N was observed, which together with the XRD and EDS (Figure S1 and Figure S3) confirmed that the Cr atoms are uniformly incorporated inside the TiO_2 microspheres. According to Figure 3 (b), the N1s core level spectrum indicates the presence of nitrogen atoms inside the TiO_2 microspheres, producing two different peaks at 396.4 and 400 eV, which have been frequently reported in the literature.[9] The peak at~396 eV is attributed to substitutionally doped nitride in the bulk, while the peak at ~400 eV is from molecular nitrogen or oxy-nitride on the surface or inside grain boundaries. The intensity of the peaks at ~396 eV for the Cr, N-doped TiO_2 is nearly double that of the N-doped TiO_2, which fitting results shows that the substitution of Ti by Cr significantly increases the solubility of the dopant nitrogen from ~2.81at.% in N-doped TiO_2 up to ~5.68 at.% in Cr,N-codoped TiO_2 under identical synthesis conditions. The most intense Ti2p peaks were located at ~458 and ~464 eV. In addition, a noticeable shoulder located in the range of 455~457 eV related to nitride was observed for N-doped and Cr, N-doped TiO_2. Clearly, introduction of Cr into TiO_2 improved the solubility of nitrogen significantly, which is in good agreement with previous reports.[11,13]

The electrical conductivity of the TiO_2, Cr-doped TiO_2, N-doped TiO_2, and Cr, N-codoped TiO_2 microspheres were measured by a

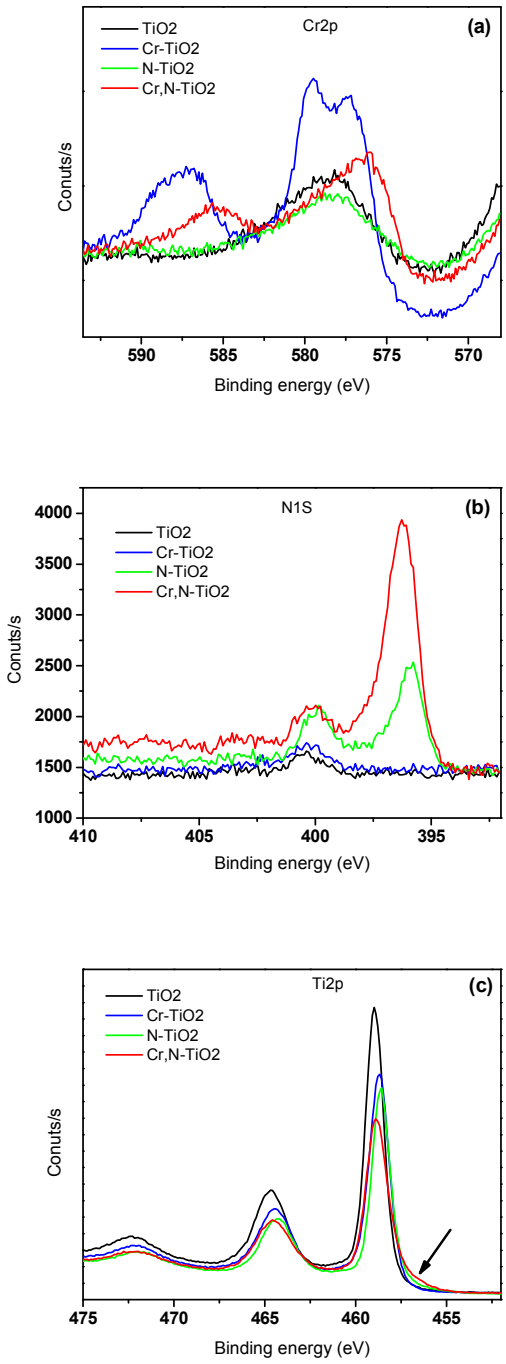

Fig. 3 X-ray photoelectron spectroscopy (XPS) spectra of pure and doped TiO_2. (a) Cr2p; (b) N1s; (c) Ti2p.

homemade two-probe conductivity apparatus, as reported in the literature,[15] and the results are shown in Figure 4. For all samples the conductivity increased with applied pressure, due to a corresponding increase in powder density. The conductivity of the pure TiO_2 microspheres was around $6.0x10^{-8}$ Scm^{-1} under a pressure of 60 MPa, which is slightly lower than the value of $7.56x10^{-8}$ Scm^{-1}

reported previously.[8] After doping with Cr, the conductivity decreased to $1.22x10^{-8}$ Scm^{-1}, which is probably due to the higher porosity and BET surface area of the Cr-doped TiO_2. After nitride, however, the conductivities under the same pressure were improved to $1.8x10^{-7}$ Scm^{-1} for N-dopedTiO_2 and to $3.05x10^{-7}$ Scm^{-1} for Cr, N-codoped TiO_2, respectively.

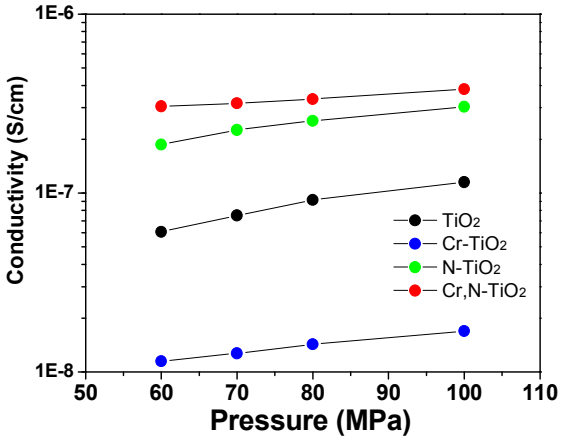

Fig. 4 Electrical conductivity of TiO_2, N-doped TiO_2, Cr-doped TiO_2 and Cr, N- codoped TiO_2 mesoporous microspheres under different pressures.

The electrochemical performances of undoped and doped TiO_2 were determined in lithium half-cells. With comparison to the electrochemical properties of pure TiO_2 reported previously, all the doped samples showed higher performance than that of pure TiO_2. For Cr-doped TiO_2, however, from Fig. S4 the capacity decreased gradually and retained only 75% of the initial capacity probably due to the low electrical conductivity and high BET surface area. Herein, in order to clarify the effect of codoping in TiO_2 on the electrochemical performance, only the results from N-doped and Cr, N-codoped TiO_2 were discussed in detail. Figure 5 (a) shows the voltage profiles of the first cycle for the N-doped and Cr, N-codoped TiO_2 in the range 1.01~2.5 V vs. Li^+/Li at a rate of 0.1 C (1C=335 $mAhg^{-1}$). For N-doped TiO_2, two distinct plateaus appear at 1.76 and 1.89 V, respectively, corresponding to lithium insertion and extraction in the anatase phase (the plateaus appear at 1.75 and 1.90 V, respectively in the undoped material). For Cr, N-codoped TiO_2, however, the discharge plateau was elevated to 1.77 V and the charge plateau dropped to 1.88 V, which indicated a slightly reduced polarization of the electrode. In addition, for the Cr, N-codoped TiO_2 the sloping region below the plateau increased, which indicated greater pseudocapacitive storage of Li in the surface area or in the pores. From Figure S4, both N-doped and Cr, N-codoped TiO_2 microsphere electrodes showed an excellent cycle life at 0.2 C; more than 94% of the capacity was retained after 100 cycles, which is comparable to the pure TiO_2 sample. In addition, the Cr-doped TiO_2 exhibited an initial coulombic efficiency of 73%, which is much lower than 80% of pure TiO_2 due to its higher BET surface area at 0.2 C. After nitridated, however, obvious improvement on the initial coulombic efficiency was observed for both N-doped and Cr, N-codoped TiO_2 with 77% and 86% at 0.2 C, respectively, is due to the presence of a thin nitridated layer that prevents the formation of a solid electrolyte layer (SEI) on the surface of TiO_2.[9] Figure 5 (b) shows the charge-discharge capacities of the N-doped and Cr, N-codoped TiO_2 mesoporous microsphere electrodes at different current rates. At high current rates, the difference in the charge-discharge capacity between the N-doped and Cr, N-codoped TiO_2 electrodes is remarkable. The Cr, N-codoped TiO_2 electrode shows enhanced rate performance with 200 $mAhg^{-1}$ at 1C, 153 $mAhg^{-1}$ at 5C and 127 $mAhg^{-1}$ at 10C, while N-doped TiO_2 enhancement of up to

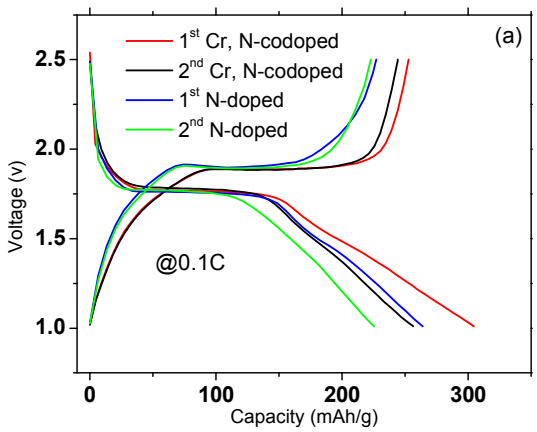

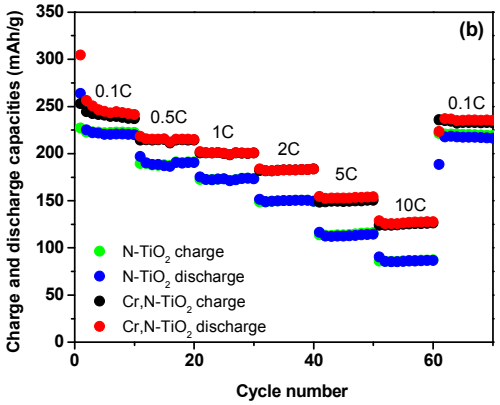

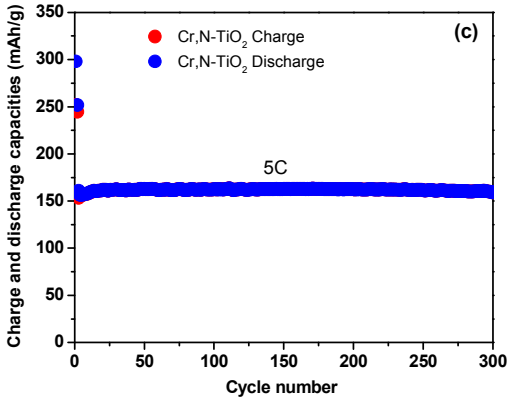

Fig. 5 (a) First and second charge and discharge voltage curves; (b) Rate performance of the N-doped TiO_2, and Cr, N- codoped TiO_2 mesoporous

microspheres electrodes; and (c) Cycling performance of the Cr, N-codoped TiO_2 mesoporous microspheres electrodes at 5C.

~50% in rate performance for Cr, N-codoped anode exhibits 173 $mAhg^{-1}$ at 1C, 114 $mAhg^{-1}$ at 5C and 87 $mAhg^{-1}$ at 10C. There is an as compared to N-doped TiO_2 at high current rates, which results mainly from the improved electronic conductivity. In order to test the cyclability at high rates, a lithium cell made by Cr, N-codoped TiO_2 microsphere material was cycled at 5 C (1675 mAg^{-1}) for 300 cycles, after aging at C/10 for 2 cycles. Figure 5(c) shows the capacity starts at 153 $mAhg^{-1}$, then gradually increases to 161 $mAhg^{-1}$, still maintain at 159.6 $mAhg^{-1}$ after 300 cycles.

To understand the effect of nitrogen doping level on the Li-ion diffusivity in N-doped and Cr, N-codoped TiO_2, cyclic voltammetry measurements were carried out at various scan rates in the range of 0.1-1.25 mVs^{-1}. The results are shown in Figure 6 (a) and (b). The Li ion diffusion coefficient was obtained using the Randles-Sevcik Equation (equation 1) at room temperature.[17]

$$I_p = 269000n^{3/2}AD^{1/2}Cv^{1/2} \quad (1)$$

In equation 1, n is the number of electrons per molecule during the intercalation, A the surface area of the anode, C the concentration of lithium ions, D the diffusion coefficient of lithium ion and v is the scan rate. A linear relationship between I_p and $v^{1/2}$ was obtained as shown in Figure 6 (c), and the diffusion coefficient of lithium ions both in N-doped and Cr, N-codoped TiO_2 microspheres were calculated according to the slopes. It was found that the diffusion coefficient of lithium in Cr, N-codoped TiO_2 (2.45×10^{-10}, and 6.702×10^{-10} cm^2s^{-1} for insertion and extraction, respectively) are around three times higher than N-doped TiO_2 (6.09×10^{-11} and 2.37×10^{-10} cm^2s^{-1} for insertion and extraction, respectively), suggesting that the increase in the electronic conductivity was beneficial for the diffusion of lithium ions. Though the measured Li diffusion coefficients of Cr, N-codoped TiO_2 were in the range of 10^{-10}~ $10^{-11}cm^2s^{-1}$, this should not limit the capacity for an average particle size of 20 nm. The mesoporous morphology allows the electrolyte to contact the surface of the nanoparticles, resulting in a short Li-ion diffusion path. Though the benefits of the morphology on Li-ion diffusion path are present for all samples, the increase in electronic conductivity is most prominent for the co-doped sample. Therefore, the improved high rate capacity could be mainly due to the increased electronic conductivity and the enhanced surface Li storage, which extends into the centre of the micron-sized spheres.

It is useful to compare the properties of codoped TiO_2 with those of the promising polymorph TiO_2-B. The TiO_2-B polymorph which is composed of edge- and corner-sharing TiO_2 octahedra that form an open framework structure, has been widely reported as an anode for Li-ion batteries.[5,9,18] It shows a favorable channel structure for lithium mobility, which results in fast charge/discharge capability of a lithium cell. It has been identified that the lithium intercalation in TiO_2-B features a pseudocapacitive process, rather than the solid-state diffusion process observed for anatase and rutile. Indeed, as in our previous report,[7] mesoporous TiO_2-B displayed excellent electrochemical properties. However, exploiting the properties of mesoporous TiO_2-B is hampered by the fact that reported synthetic approaches can be difficult, costly, provide only small quantities and in low yield, and may be difficult to scale up, since the production process of this material is complex and involves many steps. Also due to the pseudocapacitive process the charge/discharge voltage profile is sloping rather than a flat potential profile, which may lead to a more complicated battery voltage management in the battery package. This is particularly true for application in power sources. Herein, we have demonstrated a simple and promising method to

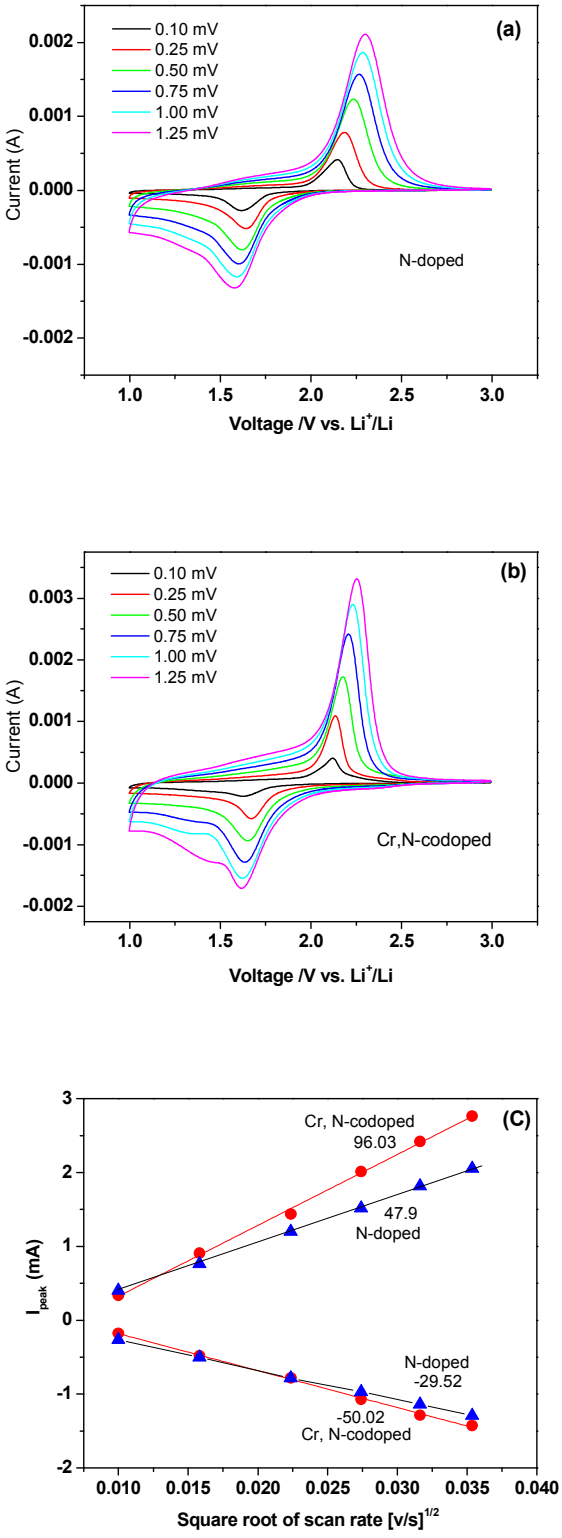

Figure 6. CV profiles of (a) N-doped TiO_2 microspheres (b) Cr, N-codoped TiO_2 microspheres with various scan rates and (c) Relationship between the peak current and the square root of scan rate in cathodic

and anodic processes for N-doped (blue) and Cr, N-codoped (red) TiO_2 microspheres.

improve the electrochemical properties of mesoporous anatase TiO_2 microspheres, using a concept of doping followed by a post annealing step.

In addition, the electronic structures, deformation charge density, dipole moment and optical properties of nitrogen and transition metal M (V, Cr, Mn, Fe, Co, Ni, Cu and Zn) codoped anatase TiO_2 have been studied using the plane wave ultrasoft pseudopotential method of density functional theory (DFT).[19] These results indicated that the calculated absorption coefficients of N, Cr-codoped TiO_2 are consistent with the experimental values. They also found that among the eight codoping pairs, Mn, N-codoped TiO_2 has the largest value of absorption efficient in the visible-light region. This indicates further scope for development of the codoping approach in enhancing the electrochemical properties of electrode materials, beyond the beneficial Cr,N-codoping presented here.

Conclusions

In summary, Cr, N-codoped TiO_2 mesoporous microspheres with enhanced electrical conductivity have been successfully synthesized by a facile hydrothermal method followed by annealing under ammonia atmosphere. For comparison between N-doped and Cr, N-codoped TiO_2 mesoporous microspheres, the latter showed greatly improved electrochemical lithium storage capacity and rate capability, due to improvement in electronic conductivity and Li-ion diffusion coefficient, which derives from an enhancement provided by the n-p dopant pair of both the thermodynamic and the kinetic solubility. Through Cr,N-codoping in TiO_2, we have successfully demonstrated a superior performance of 159.6 $mAhg^{-1}$ at 5 C with a drop of less than 1% after 300 cycles.

Acknowledgements

This work was sponsored by the Materials Sciences and Engineering Division, Office of Basic Energy Sciences, U.S. Department of Energy. Microscopy work was conducted at the ORNL SHaRE user facility, which is sponsored by the Office of Basic Energy Sciences, U.S. Department of Energy. Drs. Z. Bi and B. Guo acknowledge the support of the ORISE postdoctoral fellowship.

Notes and references

Dr. Z Bi, Dr. M. P. Paranthaman, Dr. B. Guo, Dr. C. A. Bridges, Dr. X.-G. Sun, Dr. S. Dai
Chemical Sciences Division, Oak Ridge National Laboratory
Oak Ridge, TN 37831, USA
Email: paranthamanm@ornl.gov; bridgesca@ornl.gov; biz1@ornl.gov
Dr. R. R. Unocic, H. M. Meyer III
Materials Science and Technology Division
Oak Ridge National Laboratory, Oak Ridge, TN 37831, USA

Electronic Supplementary Information (ESI) available: [details of any supplementary information available should be included here]. See DOI: 10.1039/b000000x/

1 (a) K. Kalyanasundaram, M. Gratzel, *Coordination Chemistry Reviews*, 1998, **177**, 347, (b) M. Gratzel, *Nature*, 2001, **414**, 338, (c) P. G. Bruce, B. Scrosati and J. M. Tarascon, *Angew. Chem., Int. Ed*., 2008, **47**, 2930.

2 (a) Z. G. Yang, D. Choi, S. Kerisit, K. Rosso, D. H. Wang, J. Zhang, G. Graff, J. Liu, *J. Power Sources*, 2009, **192**, 588, (b) D. H. Wang, D. W. Choi, J. Li, Z. G. Yang, Z. M. Nie, R. Kou, D. H. Hu, C. M. Wang, L. V. Saraf, J. G. Zhang, I. A. Aksay, J. Liu, *ACS Nano,* 2009, **3**, 907, (c) Y. S. Hu, L. Kienle, Y. G. Guo, J. Maier, *Adv. Mater*, 2006, **18**, 1421.

3 (a) T. P. Feist, P. K. Davies, *J Solid State Chem*., 1992, **101**, 275, (b) T. Kogure, T. Umezawa, Y. Kotani, A. Matsuda, M. Tatsumisago, T. Minami, *J. Am. Ceramic Soc*., 1999, **82**, 3248, (c) C. Wessel, L. A. Zhao, S. Urban, R. Ostermann, I. Djerdj, B. M. Smarsly, L. Q. Chen, Y. S. Hu, S. Sallard, *Chem. Eur. J*., 2011, **17**, 775.

4 (a) G. Armstrong, A. R. Armstrong, J. Canales, P. G. Bruce, *Chem. Commun.,* 2005, **19,** 2454, (b) G. Armstrong, A. R. Armstrong, J. Canales, P. G. Bruce, *Electrochem. and Solid State Lett.,* 2006, **9**, A139, (c) K. Wang, M. Wei, M. A. Morris, H. Zhou, J. Holmes, *Adv. Mater*., 2007, **19**, 3016.

5 (a) A. R. Armstrong, G. Armstrong, J. Canales, P. G. Bruce, *Angew. Chem., Int. Ed*., 2004, **43**, 2286, (b) A. R. Armstrong, G. Armstrong, J. Canales, R. Garcia, P. G. Bruce, *Adv. Mater*., 2005, **17**, 862.

6 (a) T. Beuvier, M. Richard-Plouet, M. Mancini-Le Granvalet, T. Brousse, O. Crosnier, L. Brohan, *Inorganic Chemistry*, 2010, **49**, 8457, (b) G. Zhu, Y. Wang, Y. Xia, *Energy Environ. Sci.,* 2012, **5**, 6652.

7 (a) Y. Guo, Y. Hu, J. Maier, *Chem. Commun*., 2006, **26**, 2783, (b) Z. Wang, S. Liu, G. Chen, D. Xia, *Electrochem. and Solid State Lett*., 2007, **10**, A77, (c) J. Qian, M. Zhou, Y. Cao, X. Ai, H. Yang, *J. Phys. Chem. C*, 2010, **114**, 3477, (d) S. Yoon, A. Manthiram, *J. Phys. Chem. C*, 2011, **115**, 9410, (e) H. Liu, Z. Bi, X. Sun, R. Unocic, M. Paranthaman, S. Dai, G. Brown, *Adv. Mater.,* 2011, **23**, 3450, (f) J. S. Chen, Y. L. Tan, C. M. Li, Y. L. Cheah, D. Luan, S. M. Freddy, Y. C. Boey, L. A. Archer, and X. W. Lou, *J. Am. Chem. Soc*., 2010, **132**, 6124.

8 (a) I. Moriguchi, R. Hidaka, H. Yamada, T. Kudo, H. Murakami and N. Nakashima, *Adv. Mater*., 2006, **18**, 69, (b) Y. S. Hu, Y. G. Guo, W. Sigle and J. Maier, *Adv. Mater*., 2007, **19**, 2087, (c) H. Kim, M. G. Kim, T. J. Shin, H. J. Shin and J. Cho, *Electrochem. Commun*., 2008, **10,** 1669, (d) K.-S. Park, J.-G. Kang, Y.-J. Choi, S. Lee, D.-W. Kim and J.-G. Park, *Energy Environ. Sci.,* 2011, **4,** 1796, (e) L. Kavan, R. Bacsa, M. Tunckol, P. Serp, S. M. Zakeeruddin, F. Le Formal, M. Zukalova and M. Graetzel, *J. Power Sources*, 2010, **195**, 5360, (f) L. Shen, E. Uchaker, C. Yuan, P. Nie, M. Zhang, X. Zhang, and G. Cao, *ACS Appl. Mater. Interfaces*, 2012, **4**, 2985, (g) L. Zeng, C. Zheng, L. Xia, Y. Wang and M. Wei, *J. Mater. Chem. A*, 2013, **1**, 4293.

9 (a) S. Das, M. Gnanavel, M. Patel, C. Shivakumara, A. Bhattacharya, *J. Electrochem. Soc.*, 2011, **158,** A1290, (b) Y. Wang, T. Chen, Q. Mu, *J. Mater. Chem*., 2011, **21**, 6006, (c) M. Batzill, E. Morales, U. Diebold, *Phys. Rev. Lett*., 2006, **96**, 0261031, (d) K. Han, J. Lee, Y. Kang, J. Lee, J. Kang, *Small*, 2008, **4**, 1682, (e) H. Han, T. Song, J. Bae, L. Nazar, H. Kim, U. Paik, *Energy Environ. Sci*., 2011, **4,** 4532, (f) Y. Wang, B. M. Smarsly, I. Djerdj, *Chem. Mater*, 2010, **22**, 6624. (g) S. Yoon, C. A. Bridges, R. R. Unocic, and M. Paranthaman, *J. Mater. Sci*., 2013, **48**, 5125.

10 S. B. Zhang, *J. Phys. Condens. Matter*, 2002, **14**, R881.

11 W. Zhu, X. Qiu, V. Lancu, X. Chen, H. Pan, W. Wang, N. Dimitrijevic, T. Rajh, M. Meyer III, M. Paranthaman, G. Stocks, H. Weitering, B. Gu, G. Eres, Z. Zhang, *Phys. Rev. Lett*., 2009, **103**, 226401(1).

12 (a) C. Cherian, M. Reddy, T. Magdaleno, C. Sow, K. Ramanujachary, G. V. Subba Rao, B. Chowdari, *Cryst. Eng. Comm*., 2012, **14**, 978, (b) C. Lai, X. Yuan, X. Cao, Q. Qiao, Y. Wang, S. Ye, *Electrochem. and Solid State Lett*., 2012, **15**, A65.

13 (a) Y. Li, W. Wang, X. Qiu, L. Song, M. Meyer III, M. Paranthaman, G. Eres, Z. Zhang, B. Gu, *Applied Catal. B-Environ*., 2011, **110**, 148, (b) M. Chiodi, C. Cheney, P. Vilmercati, E. Cavaliere, N. Mannella, H. Weitering, L. Gavioli, *J. Phys Chem. C*, 2012, **116**, 311.

14 (a) A.C. Larson, R.B. von Dreele, General Structure Analysis System (GSAS), Los Alamos National Laboratory Report LAUR 86748, 2000, (b) B.H. Toby, *J. Appl. Crystallogr*., 2001, **34**, 210.

15 (a) S. Mischler, H. J Mathieu, D. Landolt, *Surf. Interface Anal*., 1998, *11*, 182, (b) I. Bertoti, *Surf. Coat. Technol*., 2002, **151**, 194.

16 (a) R. Asahi, T. Morikawa, T. Ohwaki, K. Aoki, Y. Taga, *Science*, 2001, **229**, 269, (b) S. F. Chen, S. J. Zhang, W. Zhao, W. Liu, J. *Nanopart. Res*., 2009, **11**, 931.

17 (a) P. Zanello, *Inorganic Electrochemistry: Theory, Practice and Application*, The Royal Society of Chemistry 2003. ISBN 0-85404-661, (b) M. Stromme, G. A. Niklasson, C. G. Granqvist, *Solid State Commun*., 1995, **96**, 151-154.

18 (a) S. Liu, H. Jia, L. Han, J. Wang, P. Gao, D. Xu, J. Yang, S. Che, *Adv. Mater*., 2012, **24,** 3201, (b) Y. Ren, Z. Liu, F. Pourpoint, A. R.

Armstrong, C. P. Grey, P. G. Bruce, *Angew. Chem., Int. Ed*., 2012, **51,** 2164-2167.
19 R. Zhang , Q. Wang, J. Liang, Q. Li, J. Dai, W. Li, *Physica B*, 2012, **407**, 2709.